HHS Public Access

Author manuscript

Chem Commun (Camb). Author manuscript; available in PMC 2024 June 06.

Published in final edited form as:

Chem Commun (Camb). ; 59(46): 7040–7043. doi:10.1039/d3cc02186f.

Ganglioside GM1 produces stable, short, and cytotoxic $A\beta_{40}$ protofibrils

Manjeet Kumar[a], **Magdalena I Ivanova**[b], **Ayyalusamy Ramamoorthy**[a]

[a]Biophysics, Department of Chemistry, Biomedical Engineering, Macromolecular Science and Engineering, Michigan Neuroscience Institute, University of Michigan, Ann Arbor, MI 48109-1055, USA.

[b]Department of Neurology, University of Michigan, Ann Arbor, MI 48109

Abstract

Monosialoganglioside GM1-bound amyloid β-peptides have been found in patients' brains exhibiting early pathological changes of Alzheimer's disease. Herein, we report the ability of non-micellar GM1 to modulate $A\beta_{40}$ aggregation resulting in the formation of stable, short, rod-like, and cytotoxic $A\beta_{40}$ protofibrils with the ability to potentiate both $A\beta_{40}$ and $A\beta_{42}$ aggregation.

Alzheimer's disease (AD) is associated with the gradual accumulation of cross-β amyloid fibrils of $A\beta_{40}$ and $A\beta_{42}$ in brains. Protein and peptide fibrillation is not due to the direct conversion of soluble monomeric form to insoluble amyloid fibrils. Instead, multiple intermediate processes may be involved, including the formation of prefibrillar or protofibrillar species that mainly act as primary or secondary nuclei for further fibril growth.[1] These intermediate aggregates are considered to be the dominant cytotoxic forms of misfolded proteins/peptides.[2–4]

Yanagisawa et al. identified a unique GM1 ganglioside-bound Aβ species in the brains of patients with early pathological changes associated with AD.[5,6] Gangliosides, including GM1, are abundantly found in the neuronal membrane. Generally, free gangliosides are released in the extracellular region from the damaged cell membrane.[7,8] Several studies have demonstrated that ganglioside micelle, or clusters in the membrane, catalyze toxic Aβ species' formation.[9–17] Additionally, free lipids have been shown to modulate the aggregation kinetics of Aβ peptides.[18–21] This *in vitro* study is focused on unraveling the molecular processes underlying the early conformational changes of Aβ induced by the interaction with GM1, which have been linked to early AD onset. Our results show that $A\beta_{40}$ produced stable, thioflavin T (ThT)-positive, cytotoxic, rod-like structures of diameter (22.5 ± 13.1 nm) and length (38 ± 20.3 nm) in the presence of GM1. Ganglioside induced

ramamoor@umich.edu.

M.K. and A.R. designed the research, M.K. performed the experiments and processed the data, M.K., M.I. and A.R. analyzed the data, M.K., M.I. and A.R. wrote the manuscript, and A.R. directed the project.

†Electronic Supplementary Information (ESI) available: [details of any supplementary information available should be included here]. See DOI: 10.1039/x0xx00000x

Conflicts of interest

There are no conflicts to declare.

$A\beta_{40}$ species were able to catalyze the conversion of unfolded monomeric $A\beta_{40}$ and $A\beta_{42}$ to β-sheet rich structures.

The interaction of $A\beta_{40}$ with non-micellar GM1 was monitored via ThT fluorescence assay (Fig.1A). The critical micelle concentration (CMC) of GM1 used in our study was calculated to be 79.4 ± 5.6 μM (Fig.S1). *In vitro* experiments carried out at physiologically relevant pH and temperature conditions, reported the formation of $A\beta_{40}$ aggregates via a nucleation-dependent polymerization, typically displaying a sigmoidal curve with a prominent lag-phase, a growth phase, and an equilibrium phase.[22,23] Our $A\beta_{40}$ samples showed similar aggregation kinetics with a lag-phase (T_{lag}) of around 8.8 hours (h). T_{lag} for the formation of β-sheet rich species in $A\beta_{40}$ alone and GM1-containing samples were deduced from the ThT fluorescence data fitted to a sigmoidal function (Fig.1A).[24] Interestingly, there was a significant reduction in the lag-phase of $A\beta_{40}$ amyloid fibril formation and a slight increase in ThT fluorescence upon the addition of increasing concentration of GM1. A 1 μM GM1 was sufficient to reduce the lag-phase of 10 μM $A\beta_{40}$ by 4.8 h. The decrease in the lag-phase and the increase in ThT fluorescence intensity suggested an acceleration of $A\beta_{40}$ fibril formation. On the contrary, Chakravorty et al.,[18] reported the inhibition of $A\beta_{40}$ aggregation, which may be due to the use of frozen GM1 stock solution. To confirm the above observation, TEM images were acquired from 10 μM $A\beta_{40}$ after incubation for 48 hours at physiological pH and temperature in the absence (Fig.1B) and the presence of 1 μM GM1 (Fig.1C, Fig.1D). $A\beta_{40}$ alone showed the presence of typical long amyloid fibril of average diameter (10.6 ± 2.1), as previously reported.[25] However, significantly shorter, rod-like fibrillar structures of varying width (average = 22.5 ± 13.1 nm) and length (average = 38 ± 20.3 nm) were observed in GM1 modulated $A\beta_{40}$. Among the heterogeneous population of dominant short, rod-like GM1-modified $A\beta_{40}$ species, a rare long fibril, most likely of non-GM1 bound $A\beta_{40,}$ was also observed. The short, rod-like $A\beta_{40}$ filaments bind more efficiently to ThT, indicating they have similar cross-β architecture as observed in most amyloid fibrils.[26,27]

Several studies have suggested ganglioside nanoclusters in neuronal membranes induce a conformational change in $A\beta_{40}$.[28–31] So, we were interested in examining if the $A\beta_{40}$ can also undergo a secondary structure transition in the presence of GM1. Far-UV circular dichroism (CD) of 20 μM $A\beta_{40}$ in the absence and presence of 2 μM GM1, monitored over 63 h at physiological pH and temperature, did not show any change except for the decrease in random-coil content, as evidenced by the reduction of negative ellipticity peak at 198 nm (Fig.2A, Fig.2B, Fig.2C). An immediate reduction in random-coil content in $A\beta_{40}$ with no subsequent appearance of other secondary structure peaks as soon as GM1 was added suggests a fraction of $A\beta_{40}$ rapidly forms insoluble aggregates/nuclei. This may explain the reduction in the lag-phase of GM1-containing $A\beta_{40}$ in Figure 1. After that, we compared the molar ellipticity of $A\beta_{40}$ with GM1 at 198 nm to the $A\beta_{40}$ alone sample (Fig.2C, Fig.2D). Both $A\beta_{40}$ samples displayed a similar rate of change in the random coil during their aggregation. Overall, we infer that the nucleating species forming the cross-β sheet-rich structure are similar in both samples. Moreover, the apparent rate constant (k_{app}) for the formation of cross-β sheet rich species in $A\beta_{40}$ alone and GM1-containing samples were deduced from the ThT fluorescence data fitted to a sigmoidal function (Fig.1A).[24] The k_{app} for 10 μM $A\beta_{40}$ alone is 0.019/h, while the k_{app} for 10 μM $A\beta_{40}$ in the presence of

1 μM, 2.5 μM, 20 μM, and 40 μM are 0.013/h, 0.011/h, 0.012/h and 0.01/h, respectively. The comparatively similar k_{app} for GM1-containing $A\beta_{40}$ and the absence of long fibrillar species (Fig.1C) compared to $A\beta_{40}$ alone suggested that GM1 inhibited the elongation of $A\beta_{40}$ fibrils.

The ThT, TEM imaging, and far-UV CD results confirm that the short, rod-like $A\beta_{40}$ species generated upon interaction with GM1, is an on-pathway stable intermediate, most likely protofibrils of fully matured fibrils of $A\beta_{40}$. Interestingly, metastable protofibril of Aβ with the ability to alter the electrical activity of neurons, causing neuronal loss, has been reported earlier.[32–34] We, therefore, performed a cell viability assay on differentiated human neuroblastoma SH-SY5Y cells treated with samples containing $A\beta_{40}$ fibril, GM1-modulated $A\beta_{40}$ protofibril, and GM1 alone (Fig.3). Sample containing 10 μM $A\beta_{40}$ fibril alone did not show any significant cell cytotoxicity on differentiated SH-SY5Y cells, as reported earlier.[35] However, we observed approximately 33% less cellular metabolic activity from differentiated SH-SY5Y cells upon incubation with GM1-induced $A\beta_{40}$ protofibrils. A 1 μM GM1 (alone) incubated for 48 h showed no cell death. This observation implies that $A\beta_{40}$ protofibrils are potentially cytotoxic.

Apart from the direct toxic effect displayed by the intermediates of many amyloid-forming proteins, as observed in this study, aggregating proteins can catalyze the conversion of other amyloid or neighboring proteins/peptides to aggregates[36]. The formation of amyloid fibrils from normal functional, misfolded, or unfolded proteins mostly follows nucleation-dependent polymerization similar to crystallization.[37,38] The critical step in these processes is the generation of the smallest unit, often termed nuclei (seeds), that can promote the formation of amyloids by rapidly converting non-aggregated proteins/peptides into fibrils.[33] There are two types of polymerization: homogenous polymerization, where both the nuclei and precursor proteins/peptides are the same, and heterogeneous polymerization (cross-seeded),[39] in which the nuclei of one protein/peptide seed the aggregation of a different protein/peptide. Apart from primary nucleation, secondary nucleation, generally surface-catalyzed conversion of proteins/peptides to amyloid fibrils, can also lead to fibril proliferation.[40] The rapid transformation of non-aggregated proteins/peptides through primary and secondary nucleation has been established as a central process explaining the “infectious” nature of prion proteins in prion diseases and the spread of pathogenic inclusions in many neurodegenerative disorders, including AD.[41–43] Knowing the importance of nucleation in AD, we studied whether GM1-induced $A\beta_{40}$ protofibril can catalyze the conversion of $A\beta_{40}$ and $A\beta_{42}$ (second major isomer generated from amyloid precursor protein involved in AD pathogenesis) to β-sheet rich structure. For seeding and cross-seeding experiments, we prepared the $A\beta_{40}$ seeds by incubating 10 μM $A\beta_{40}$ in the absence and presence of 1 μM GM1, without ThT dye in the amyloid-forming condition as described in the materials and method section (see the supplementary information). Using the ThT fluorescence assay, we studied the secondary nucleation process of $A\beta_{40}$ by adding varying amounts of preformed $A\beta_{40}$ fibril to 5 μM of monomeric $A\beta_{40}$ under the quiescent condition at physiological pH and temperature (Fig.4A). Addition of 1%, 2.5% and 5% v/v preformed fibril as seed, significantly reduced the lag-phase of 5 μM $A\beta_{40}$ aggregation kinetics. Meanwhile, additions of 1%, 2.5%, and 5% v/v preformed $A\beta_{40}$ fibril to 5 μM of monomeric $A\beta_{42}$ led to a spontaneous increase in ThT fluorescence,

suggesting immediate $A\beta_{42}$ fibril formation (Fig.4B). Seeding and cross-seeding of $A\beta_{40}$ and $A\beta_{42}$ respectively has earlier been observed with sonicated $A\beta_{40}$ fibril.[44] However, our study used unsonicated $A\beta_{40}$ fibril as seeds. Similar to the secondary nucleation observed with $A\beta_{40}$ fibril (Fig.4A, Fig.4B), the addition of preformed GM1-induced $A\beta_{40}$ protofibril as seed (1%, 2.5% and 5% v/v) significantly reduced the lag-phase of 5 μM $A\beta_{40}$ aggregation kinetics. Additionally, $A\beta_{40}$ aggregates formed in the presence of GM1-induced $A\beta_{40}$ protofibril bound more efficiently to ThT as indicated by higher ThT fluorescence intensity (Fig.4C). Furthermore, an immediate rise in ThT fluorescence was observed upon the addition of varying amounts of GM1-induced $A\beta_{40}$ protofibril to 5 μM of monomeric $A\beta_{42}$, which had a prominent lag-phase of ~2 h without the seed (Fig.4D). That is, GM1-induced $A\beta_{40}$ protofibril also catalyzed the aggregation of monomeric $A\beta_{40}$ and $A\beta_{42}$. As summarized in supplementary figure S2, we have shown the formation of short, rod-like intermediate of $A\beta_{40}$, exceptionally stable protofibrils structure of average length of less than 40 nm upon interaction with ganglioside GM1. The GM1-induced $A\beta_{40}$ protofibril reduced the viability of human neuroblastoma cells, SHSY5Y. Several studies, as mentioned earlier, and reviewed by Matsuzaki[9], have shown that the interaction of GM1 in micellar or nanocluster forms with $A\beta_{40}$ brings about an immediate α-helix/β-sheet conformational change leading to the formation of toxic, long fibrillar amyloid-β species. However, our study found that non-micellar GM1 produces stable, toxic $A\beta_{40}$ protofibrils of less than 40 nm size without undergoing α-helical transition upon interaction with the peptide. Potential implications of novel $A\beta_{40}$ species reported in this study include: GM1-bound $A\beta_{40}$ may be secreted efficiently due to its stability and smaller size into the extracellular space and act as a “seed” for amyloid-forming proteins/peptides, leading to a large-scale aggregation, apart from having a direct toxic effect to cells.[45,46] Thus, our findings may explain the molecular basis for the early pathological changes observed in some patients with AD. In hindsight, the generation of stable, neurotoxic, protofibrillar assemblies of $A\beta_{40}$ exhibiting prion-like properties to seed the aggregation of other proteins could contribute more to the neurodegeneration than the other observed oligomeric and amyloid fibrils. From a therapeutic perspective, blocking the formation of stable intermediates resembling those described here could successfully combat neurodegenerative diseases, including AD.

Supplementary Material

Refer to Web version on PubMed Central for supplementary material.

Acknowledgment

This study was supported by the National Institutes of Health Grants (AG048934 and DK13221401 to A.R.).

Notes and references

1. Chiti F and Dobson CM, Annu Rev Biochem, 2006, 75, 333–366. [PubMed: 16756495]
2. Hardy J and Selkoe DJ, Science, 2002, 297, 353–356. [PubMed: 12130773]
3. Glabe CC, Subcell Biochem, 2005, 38, 167–177. [PubMed: 15709478]
4. Nguyen PH, Ramamoorthy A, Sahoo BR, Zheng J, Faller P, Straub JE, Dominguez L, Shea JE, Dokholyan N. v., de Simone A, Ma B, Nussinov R, Najafi S, Ngo ST, Loquet A, Chiricotto M, Ganguly P, McCarty J, Li MS, Hall C, Wang Y, Miller Y, Melchionna S, Habenstein B, Timr S,

Chen J, Hnath B, Strodel B, Kayed R, Lesné S, Wei G, Sterpone F, Doig AJ and Derreumaux P, Chem Rev, 2021, 121, 2545–2647. [PubMed: 33543942]

5. Yanagisawa K, Odaka A, Suzuki N and Ihara Y, Nat Med, 1995, 1, 1062–1066. [PubMed: 7489364]
6. Yanagisawa K and Ihara Y, Neurobiol Aging, 1998, 19, S65–S67. [PubMed: 9562471]
7. Sastry PS, Prog Lipid Res, 1985, 24, 69–176. [PubMed: 3916238]
8. Davidsson P, Wallin A, Fredman P, Gottfries CG, Karlsson I, Månsson JE, Svennerholm L and Blennow K, Arch Neurol, 1991, 48, 1032–1035. [PubMed: 1929894]
9. Matsuzaki K, Biochim Biophys Acta Biomembr, DOI:10.1016/J.BBAMEM.2020.183233.
10. Fukunaga S, Ueno H, Yamaguchi T, Yano Y, Hoshino M and Matsuzaki K, Biochemistry, 2012, 51, 8125–8131. [PubMed: 23009396]
11. Okada T, Ikeda K, Wakabayashi M, Ogawa M and Matsuzaki K, J Mol Biol, 2008, 382, 1066–1074. [PubMed: 18692507]
12. Ogawa M, Tsukuda M, Yamaguchi T, Ikeda K, Okada T, Yano Y, Hoshino M and Matsuzaki K, J Neurochem, 2011, 116, 851–857. [PubMed: 20831659]
13. Okada T, Wakabayashi M, Ikeda K and Matsuzaki K, J Mol Biol, 2007, 371, 481–489. [PubMed: 17582434]
14. Saha J, Bose P, Dhakal S, Ghosh P and Rangachari V, Biochemistry, 2022, 61, 2206–2220. [PubMed: 36173882]
15. Matsuzaki K, Kato K and Yanagisawa K, Prog Mol Biol Transl Sci, 2018, 156, 413–434. [PubMed: 29747822]
16. Matsuzaki K, Kato K and Yanagisawa K, Biochim Biophys Acta, 2010, 1801, 868–877. [PubMed: 20117237]
17. Kakio A, ichi Nishimoto S, Yanagisawa K, Kozutsumi Y and Matsuzaki K, Biochemistry, 2002, 41, 7385–7390. [PubMed: 12044171]
18. Chakravorty A, McCalpin SD, Sahoo BR, Ramamoorthy A and Brooks CL, J Phys Chem Lett, 2022, 13, 9303–9308. [PubMed: 36174129]
19. Korshavn KJ, Satriano C, Lin Y, Zhang R, Dulchavsky M, Bhunia A, Ivanova MI, Lee YH, la Rosa C, Lim MH and Ramamoorthy A, J Biol Chem, 2017, 292, 4638–4650. [PubMed: 28154182]
20. Dahse K, Garvey M, Kovermann M, Vogel A, Balbach J, Fändrich M and Fahr A, J Mol Biol, 2010, 403, 643–659. [PubMed: 20851128]
21. Sciacca MF, Lolicato F, Tempra C, Scollo F, Sahoo BR, Watson MD, García-Viñuales S, Milardi D, Raudino A, Lee JC, Ramamoorthy A and la Rosa C, ACS Chem Neurosci, 2020, 11, 4336–4350. [PubMed: 33269918]
22. Meisl G, Kirkegaard JB, Arosio P, Michaels TCT, Vendruscolo M, Dobson CM, Linse S and Knowles TPJ, Nature Protocols 2016 11:2, 2016, 11, 252–272.
23. Sahoo BR, Cox SJ and Ramamoorthy A, Chem Commun (Camb), 2020, 56, 4627. [PubMed: 32300761]
24. Morris AM, Watzky MA and Finke RG, Biochimica et Biophysica Acta (BBA) - Proteins and Proteomics, 2009, 1794, 375–397. [PubMed: 19071235]
25. Wang J, Yamamoto T, Bai J, Cox SJ, Korshavn KJ, Monette M and Ramamoorthy A, Chemical Communications, 2018, 54, 2000–2003. [PubMed: 29411841]
26. Khurana R, Coleman C, Ionescu-Zanetti C, Carter SA, Krishna V, Grover RK, Roy R and Singh S, J Struct Biol, 2005, 151, 229–238. [PubMed: 16125973]
27. Biancalana M and Koide S, Biochim Biophys Acta Proteins Proteom, 2010, 1804, 1405–1412.
28. Okada T, Wakabayashi M, Ikeda K and Matsuzaki K, J Mol Biol, 2007, 371, 481–489. [PubMed: 17582434]
29. Matsubara T, Yasumori H, Ito K, Shimoaka T, Hasegawa T and Sato T, Journal of Biological Chemistry, 2018, 293, 14146–14154. [PubMed: 30018137]
30. Matsubara T, Nishihara M, Yasumori H, Nakai M, Yanagisawa K and Sato T, Langmuir, 2017, 33, 13874–13881. [PubMed: 29148800]
31. Okada Y, Okubo K, Ikeda K, Yano Y, Hoshino M, Hayashi Y, Kiso Y, Itoh-Watanabe H, Naito A and Matsuzaki K, ACS Chem Neurosci, 2019, 10, 563–572. [PubMed: 30346704]

32. Hartley DM, Walsh DM, Ye CP, Diehl T, Vasquez S, Vassilev PM, Teplow DB and Selkoe DJ, J Neurosci, 1999, 19, 8876–8884. [PubMed: 10516307]
33. Walsh DM, Lomakin A, Benedek GB, Condron MM and Teplow DB, Journal of Biological Chemistry, 1997, 272, 22364–22372. [PubMed: 9268388]
34. Harper JD, Wong SS, Lieber CM and Lansbury PT, Biochemistry, 1999, 38, 8972–8980. [PubMed: 10413470]
35. Krishtal J, Bragina O, Metsla K, Palumaa P and Tõugu V, PLoS One, DOI:10.1371/JOURNAL.PONE.0186636.
36. Ivanova MI, Lin Y, Lee YH, Zheng J and Ramamoorthy A, Biophys Chem, DOI:10.1016/J.BPC.2020.106507.
37. Chatani E and Yamamoto N, Biophys Rev, 2018, 10, 527–534. [PubMed: 29214606]
38. Jarrett JT and Lansbury PT, Cell, 1993, 73, 1055–1058. [PubMed: 8513491]
39. Tang Y, Zhang D, Gong X, Zheng J, Tang Y, Zhang D, Zheng J and Gong X, Adv Funct Mater, 2022, 32, 2208022.
40. Törnquist M, Michaels TCT, Sanagavarapu K, Yang X, Meisl G, Cohen SIA, Knowles TPJ and Linse S, Chemical Communications, 2018, 54, 8667–8684. [PubMed: 29978862]
41. Walker LC, Schelle J and Jucker M, Cold Spring Harb Perspect Med, DOI:10.1101/CSHPERSPECT.A024398.
42. Prusiner SB, Science, 2012, 336, 1511–1513. [PubMed: 22723400]
43. Arosio P, Knowles TPJ and Linse S, Physical Chemistry Chemical Physics, 2015, 17, 7606. [PubMed: 25719972]
44. Tran J, Chang D, Hsu F, Wang H and Guo Z, FEBS Lett, 2017, 591, 177. [PubMed: 27981583]
45. Yanagisawa K, Asami-Odaka A, Suzuki N and Ihara Y, Ann N Y Acad Sci, 1996, 786, 184–194. [PubMed: 8687018]
46. Hayashi H, Kimura N, Yamaguchi H, Hasegawa K, Yokoseki T, Shibata M, Yamamoto N, Michikawa M, Yoshikawa Y, Terao K, Matsuzaki K, Lemere CA, Selkoe DJ, Naiki H and Yanagisawa K, Journal of Neuroscience, 2004, 24, 4894–4902. [PubMed: 15152051]

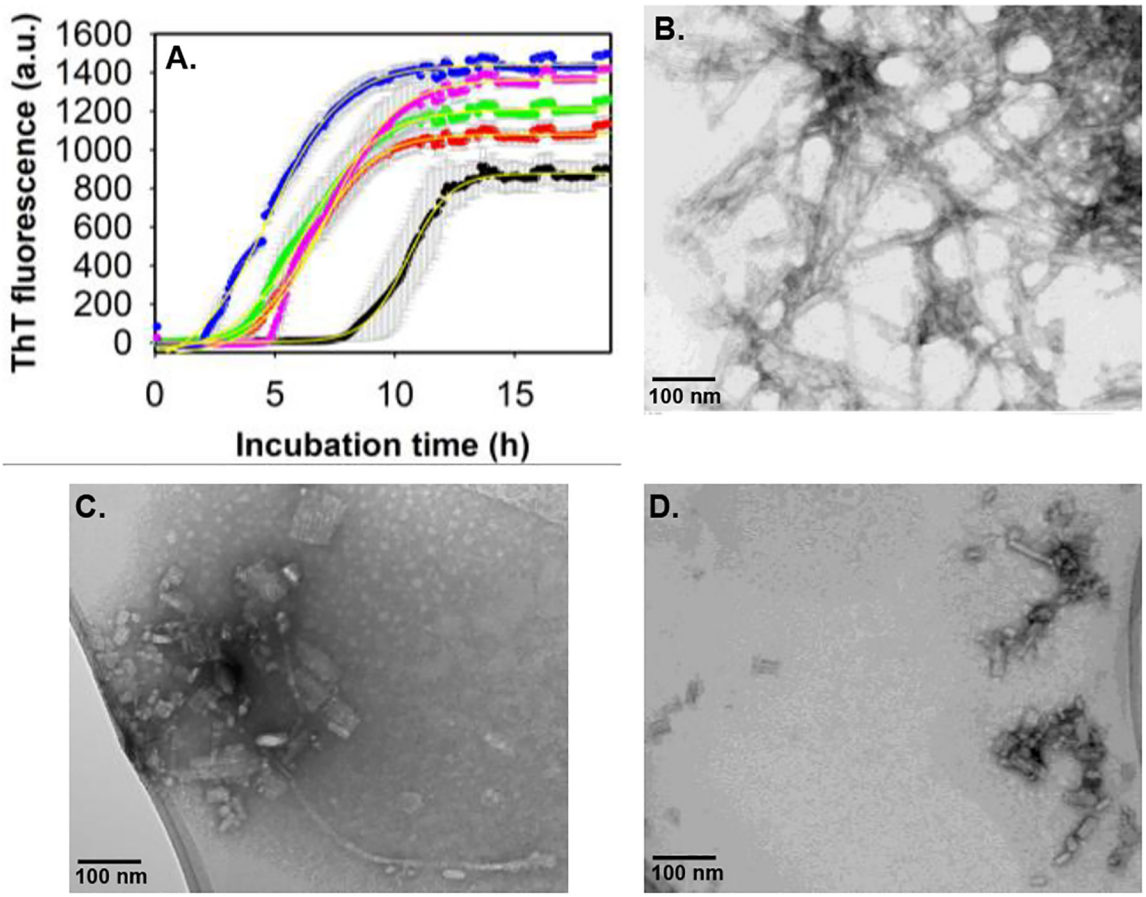

Figure 1. Probing the interaction between Aβ40 and GM1.

(A) ThT fluorescence intensity of 10 μM Aβ40 alone (black) and with varying concentrations of GM1: 1 μM (red), 2.5 μM (green), 20 μM (magenta) and 40 μM (blue) in 20 mM phosphate buffer, pH 7.4 at 37° C, slow continuous shaking. The line of best fit (yellow, R^2 =0.99) through the data points was obtained by global fitting the data with a sigmoidal function.[24] TEM images of 10 μM Aβ40 alone (B), and in the presence of 1 μM GM1 (C, D), acquired after 48 h incubation at physiological pH and temperature conditions. (C) and (D) are the images of the same sample taken from two different positions in the TEM grid. Scale bars, as indicated. All other details are given in the supporting information.

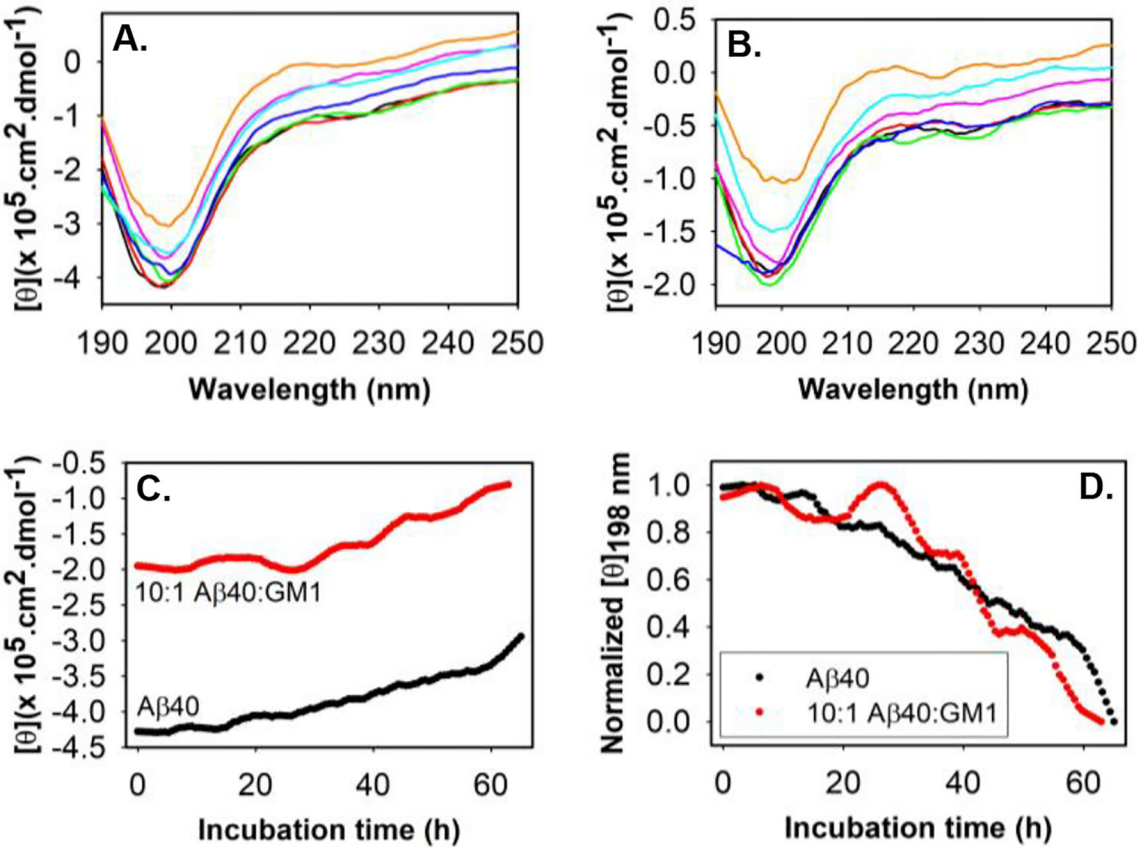

Figure 2. Comparing the rate of secondary structure change in Aβ40 during fibrillation in the absence and presence of GM1 via far-UV CD.

Molar ellipticity of 20 μM Aβ40 (A) and 20 μM Aβ40 + 2 μM GM1 (B) measured over a period of about 63 h: black (0 h), red (10 h), green (20 h), blue (30 h), magenta (40 h), cyan (50 h) and mustard (65 h). Samples were measured in 20 mM phosphate buffer, pH 7.4 at 37° C. (C) Molar ellipticity of 20 μM Aβ40 (black) and 20 μM Aβ40 + 2 μM GM1 (red) at 198 nm over a period of ~63 h. (D) Normalized molar ellipticity at 198 nm of Aβ40 in the absence and presence of GM1 as indicated. All other details are provided in the supplementary information.

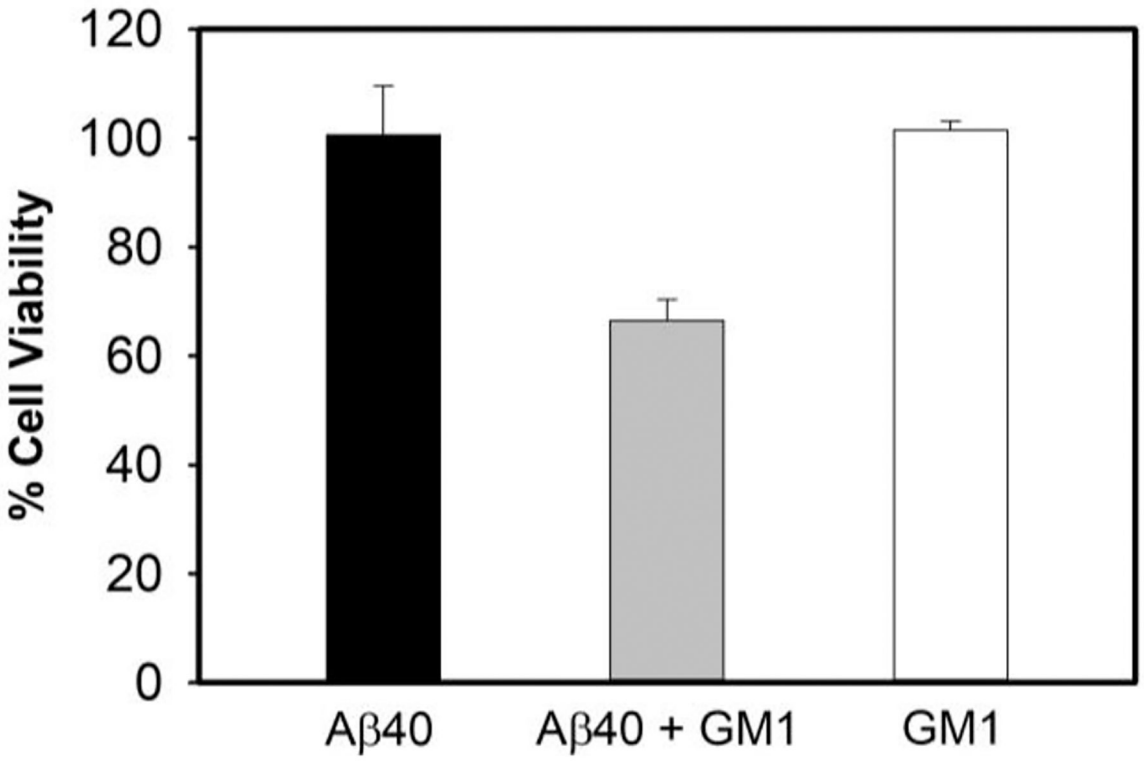

Figure 3. Evaluation of GM1-induced Aβ40 protofibril cytotoxicity.

The MTT assay was used to measure differentiated human neuroblastoma SH-SY5Y cellular metabolic activity as an indicator of cell viability upon treatment with solutions containing 10 μM Aβ40 species without (black) and with (grey) 1 μM GM1 after 2 days of incubation. The white bar is of 2-day old 1 μM GM1 alone. Data is presented as the average ± standard error, calculated from 5 replicates (n = 5). Kruskal-Wallis test indicate that the result is significant at $p < 0.05$. See the supporting information for additional details.

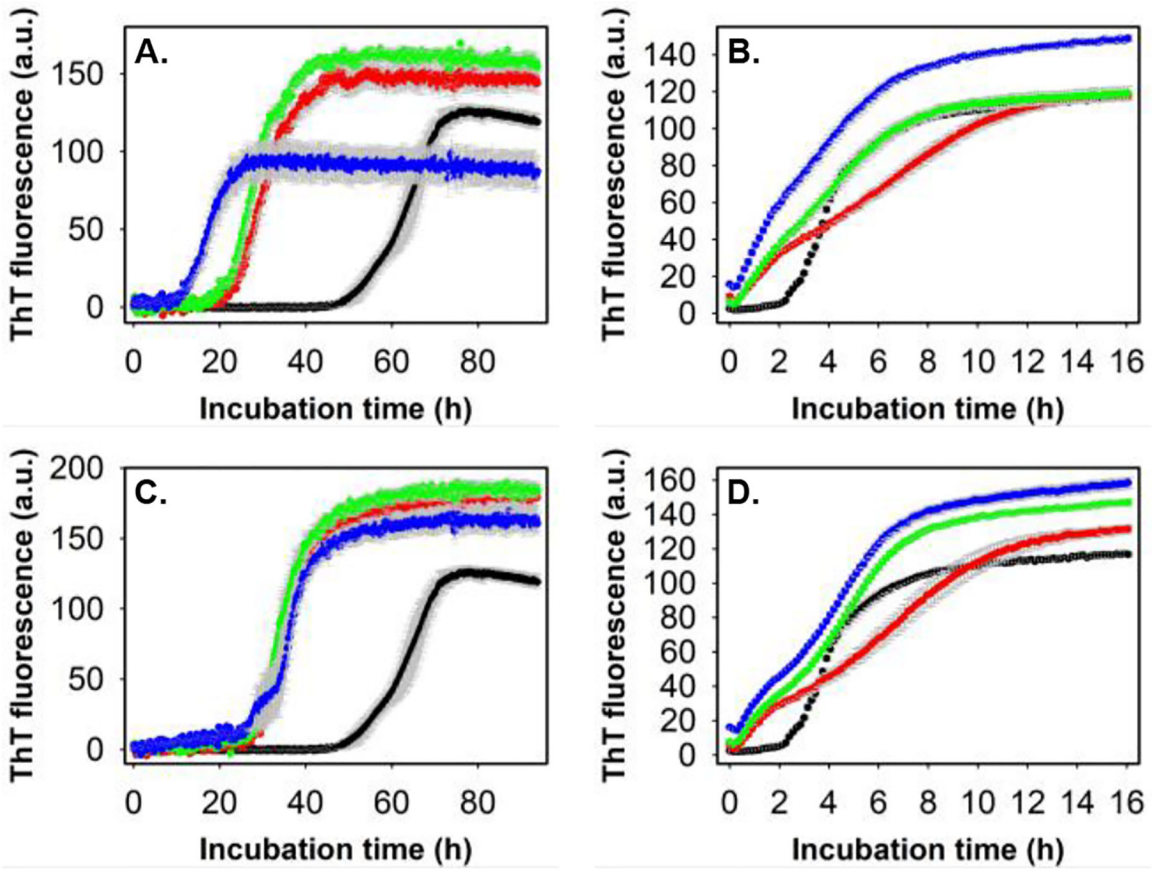

Figure 4. Seeding and cross-seeding of Aβ40 and Aβ42 with pre-formed Aβ40 aggregates.

(A) ThT fluorescence profiles of 5 μM Aβ40 alone (black) and in the presence of 1% v/v (red), 2.5% v/v (green) and 5% v/v (blue) pre-formed Aβ40 amyloid fibril in 20 mM phosphate buffer, pH 7.4, 37° C under quiescent condition. (B) ThT fluorescence profiles of 5 μM Aβ42 alone (black) and in the presence of 1% v/v (red), 2.5% v/v (green) and 5% v/v (blue) pre-formed Aβ40 amyloid fibril in 20 mM phosphate buffer, pH 7.4, 37° C under quiescent condition. (C) ThT fluorescence profiles of 5 μM Aβ40 alone (black circle) and in the presence of 1% v/v (red circle), 2.5% v/v (green circle) and 5% v/v (blue circle) pre-formed GM1-induced Aβ40 protofibril in aforementioned conditions. (D) ThT fluorescence profiles of 5 μM Aβ42 alone (black circle) and in the presence of 1% v/v (red circle), 2.5% v/v (green circle) and 5% v/v (blue circle) pre-formed GM1-induced Aβ40 protofibril in above mentioned conditions. Appropriate blank was subtracted in each case. See the supporting information for additional details.